MATERIALS CHEMISTRY FRONTIERS

RESEARCH ARTICLE

View Article Online
View Journal | View Issue

Cite this: *Mater. Chem. Front.*, 2023, 7, 2896

Constructing a new platform for photo-peroxidase catalysis: ZIF-90 as a dual 'modulator' to overcome peroxide industrial application bottlenecks†

Ke-Xin Li,[a] Guo-Wei Guan,[a] Ling-Min Pei[b] and Qing-Yuan Yang *[a]

Received 29th December 2022,
Accepted 29th March 2023

DOI: 10.1039/d2qm01371a

rsc.li/frontiers-materials

Since peroxidases have potential applications as biocatalysts, it is important to improve their usefulness. Traditional "semiconductor photocatalyst + peroxidase" catalytic cascade systems are inspired by nature's photosynthesis and provide the basis for maintaining the optimal stability and reactivity of the peroxidase enzyme. However, inherent fragility, non-recyclability, and low catalytic efficiency still limit their industrial application. In this work, we present a new generation of photoperoxidase catalytic platform, g-C_3N_4/PDI-HRP@ZIF-90 (graphite carbon nitride; PDI: perylene diimide; and HRP: horseradish peroxidase), for efficient photo-peroxidase catalysis. This new composite catalyst was created by introducing a rationally designed metal–organic framework (ZIF-90) *in situ* as a dual "modulator" for the "semiconductor photocatalyst + peroxidase" catalytic cascade system, which is highly applicable to industrial applications. *In situ* introduced modulators of ZIF-90 not only significantly increase the electron transfer rate but also significantly improve enzyme stability, cyclability, and molecular transfer rates between photoenzyme catalytic systems through spatial confinement. The new catalytic system (semiconductor + MOF + peroxidase) is capable of responding to a cascade catalytic reaction with wavelengths > 420 nm and is resistant to a catalytic environment at pH = 3. This work outlines a versatile and effective strategy to use the properties of MOFs to improve two major drawbacks of the efficient industrial use of peroxidases (inefficiency and poor stability), paving the way for efficient green biomanufacturing industrialization using peroxidases.

Introduction

Photosynthesis utilizes the Earth's most desirable energy source, sunlight, to convert CO_2 and H_2O into organics through a series of complex biochemical reactions, which provide the basis for organisms to survive in nature.[1] In this process, a number of biological enzymes are involved in catalytic reactions.[2] Enzymes are naturally derived catalysts that are highly efficient, involve mild catalytic environments and exhibit high specificity compared to traditional catalysts; due to these properties, an increasing number of challenging reactions have been attempted using biological enzymes as catalysts for chemical reactions.[3] The talented peroxidases (EC 1.11) are widely distributed in nature. They play an important role in the Animalia, Plantae and microbial kingdoms.[4] These peroxidases have a variety of applications in chemistry, such as the degradation of pollutants/wastes, asymmetric synthesis, drug synthesis and organic/polymer synthesis.[5] In contrast to oxygenases that utilize nonreactive molecular O_2 to oxidize substrates, peroxidases are heme proteins that oxidize a variety of substrates by catalyzing H_2O_2 or other oxides. However, the hydroxyl radicals generated by the Fenton reaction are toxic to peroxidases when in excess.[4] Thus, the *in situ* addition of H_2O_2 is crucial for efficiently utilizing peroxidases.[6] Learning from photosynthesis in nature, second-generation photoperoxidase catalysis uses sunlight as an energy source for the *in situ* generation of H_2O_2 in peroxidase catalytic applications, which is an ideal "*ab initio*" catalytic strategy.[7–9]

The "photoperoxidase" cascade has been widely researched, in which the photocatalytic effect directly affects the range of cascade reactions that occur.[10] In general, photocatalysts involve a wider wavelength range of absorbed light and higher visible light utilization (approximately 50% of sunlight is visible light), and the slower the electron–hole recombination rate is, the greater the probability that cascade reactions will occur under actual sunlight.[11,12] Peroxidases, as proteins, are not compatible with efficient photocatalytic conditions and are inherently fragile.[13] Therefore, we attempted to overcome the incompatibility of the two catalytic systems, inefficiency of the photocatalysis system and instability of the peroxidase catalytic system in conventional photoenzyme catalytic systems by introducing a

[a] School of Chemical Engineering and Technology, Xi'an Jiaotong University, Xi'an 710049, China. E-mail: qingyuan.yang@xjtu.edu.cn
[b] School of Medicine, Xizang Minzu University, Xianyang 712082, China

† Electronic supplementary information (ESI) available. See DOI: https://doi.org/10.1039/d2qm01371a

"modulator". However, the choice of modulator material and the method of combining the modulator with the photocatalyst and enzyme are worth investigating in the photoperoxidase catalytic system.[14,15] To deal with the above, Chen *et al.* modified the surface of semiconductor photocatalyst TiO_2 by phase-transitioned lysozyme (PTL) and then used a DNA helix to connect peroxidase on TiO_2.[16] Simsek *et al.* immobilized peroxidase on the surface of the semiconductor photocatalyst g-C_3N_4 by covalent bonding and physical adsorption.[17] Guo *et al.* used the classical metal–organic framework material NH_2-MIL-125 to make photo-immobilized enzyme platforms.[18] However, problems such as low visible light utilization, poor compatibility, poor stability and inflexibility still occur in the above photoperoxidase platforms. It is a promising vision to enhance the practicality of the photoperoxidase platform through modification and to extend the application of photoperoxidase catalysis from the laboratory to an industrial scale. Metal organic framework materials (MOFs) have attracted much attention from researchers as promising photocatalyst modification materials and enzyme immobilization carriers due to their large specific surface area, good optical effect, high stability and biocompatibility.

To achieve that vision, we introduced a functional material, ZIF-90, as a dual modulator to a conventional photoperoxidase system (Fig. 1). A semiconductor g-C_3N_4/PDI was selected as the photocatalyst, while a common horseradish peroxidase enzyme was selected as the model enzyme. Validated using the structural morphology, electrochemical properties, catalytic activity, stability, and practicality, ZIF-90 can modify the energy gap of g-C_3N_4/PDI (from 2.91 eV to 2.77 eV), allowing photocatalytic reactions at wavelengths higher than 420 nm and improving the catalytic efficiency of the photoperoxidase system. ZIF-90 also significantly enhances the stability and reusability of the "photoperoxidase" system by framework protection (especially against acidic environments; the catalytic activity is twice as high at pH = 3 as at pH = 7). ZIF-90 achieves the goal of transferring photoperoxidase catalysis outside of the laboratory through both energy band modulation and enzyme protection, and we have demonstrated its usefulness in sunlight degradation of three dyes (CV, CR, and RBBR). Indeed, the original intention behind the design of this platform was to provide potential for all peroxidases: the direct use of sunlight to catalyze more meaningful reactions under industrial conditions.

Experimental section

Materials

All chemicals were obtained commercially and used without additional purification. Melamine (98%), 1,2,4,5-benzenetetracarboxylic anhydride (PMDA, 98%), zinc nitrate hexahydrate (Zn(NO3)2·6H2O, 98%), imidazole-2-carboxaldehyde (ICA, 98%), polyvinylpyrrolidone (PVP, M_W: 40 000), 2,2′-azinobis(3-ethylbenzothiazoline-6-sulfonic acid ammonium salt (ABTS, 98%), basic violet 3 (CV), direct red 28 (CR), reactive blue 19 (RBBR), *N*-hydroxysulfosuccinimide sodium salt (NHS), 1-(3-dimethylaminopropyl)-3-ethylcarbodiimide (EDC), and fluorescein isothiocyanate (FI-TC) were purchased from Shanghai Aladdin Biochemical Technology Co., Ltd. Horseradish peroxidase (HRP, RZ $\geq$ 3) was purchased from Hefei Bomei Biotechnology Co. Ltd. Phosphate buffer saline (PBS, 1X) and hydrochloric acid (HCl, 37%) were purchased from Sinopharm Chemical Reagent Co. Ltd. Bradford reagent was purchased from Beijing Comwin Biotech Co. Ltd.

Instruments

The crystal structures of the materials were investigated by powder X-ray diffraction (PXRD, Bruker D8 Advance, Bruker, Germany). Vibration spectroscopy of the materials was performed by Fourier transform infrared spectroscopy (FTIR, Nicolet iS50, Thermo Fisher Scientific, China). Scanning electron microscopy (SEM, GeminiSEM 500, Carl Zeiss, China) was used to identify the morphology and particle size of the products. The presence and spatial location of HRP in the composite was identified using a super-resolution confocal microscope (Leica TCS SP8 STED 3X, Leica, Germany). Thermogravimetric analysis (TGA) was carried out

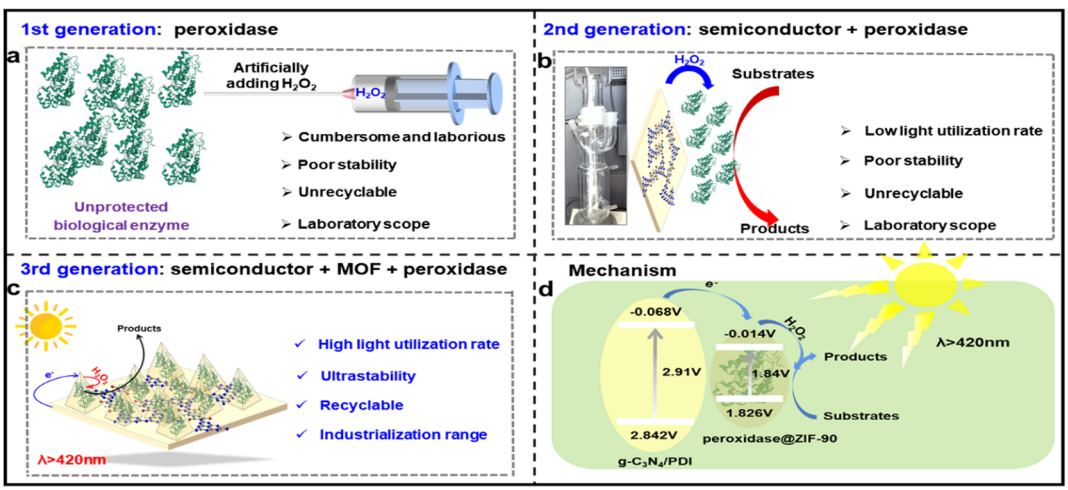

Fig. 1 (a)–(c) The different generations of the peroxidase platform; (d) the catalytic mechanism of the sunlight-immobilized peroxidase catalytic platform.

on a thermogravimetric analyzer (STA449F5, Netzsch, Germany) in the 0–800 °C range under an air atmosphere (heating rate 10 °C min^{-1}). The product concentration and sample absorbance characteristics were measured using an ultraviolet-visible-near infrared spectrophotometer (UV, PE Lambda950, SOUNDKING-DOMLTD, China). X-ray photoelectron spectroscopy (XPS) analysis was conducted with a Thermo Fisher ESCALAB Xi+ (America) X-ray photoelectron spectrometer equipped with an Al Ka X-ray radiation source. The electrochemical impedance spectroscopy (EIS) spectra, Mott–Schottky (M–S) curves, and photocurrent were obtained using a PARSTAT MS potentiostat.

Preparation of MA and g-C_3N_4/PDI

Descriptions of the MA and g-C_3N_4/PDI synthetic methods are reported in the ESI.†

Preparation of *x*%-CPZH, ZIF-90@HRP and ZIF-90

g-C_3N_4/PDI@ZIF-90@HRP with different g-C_3N_4/PDI concentrations (33.3%, 50%, 100%, 400%) was obtained by modifying the quantity of g-C_3N_4/PDI (noted as *x*%-g-C_3N_4/PDI@HRP@ZIF-90; abbreviations *x*%-CPZH).[19]

Different quantities of g-C_3N_4/PDI were mixed with 187.6 mg $Zn(NO_3)_2{\cdot}6H_2O$ in 1.5 mL D.I. water and sonicated overnight to modify Zn^{2+} on g-C_3N_4/PDI as solution A. ICA (240 mg), 25 mg of PVP and 10 mg of HRP were dissolved fully in 12.5 mL of D.I. water as solution B.[20,21]

Then, solution A was slowly poured into solution B and stirred vigorously for 30 min. The *x*%-CPZH was obtained by centrifugation, washed three times with D.I. water and dried under vacuum (Fig. 2).[22]

ZIF-90@HRP and ZIF-90 were synthesized using the same method as above, except that g-C_3N_4/PDI or g-C_3N_4/PDI and HRP were not added.[23,24]

The catalytic activity of *x*%-CPZH

HRP can catalyze the conversion of the ammonium salt of ABTS to a cation that readily disproportionates (green color, absorption wavelength at 500–900 nm). Therefore, the catalytic activity of *x*%-CPZH was obtained by testing the UV absorption intensity at 500–900 nm.[25]

Stability and reusability tests

As above, the catalytic activities of 50%-CPZH and HRP were tested by UV absorption intensity at different acidic pH values (3–7) and different temperatures (25 °C, 40 °C, 60 °C). The stability of 50%-CPZH and HRP in extreme environments was compared with relative activity. The reusability of 50%-CPZH was investigated by UV absorption intensity at 500–900 nm, 5 times.[26]

Sunlight catalytic dye degradation capacity determination

Using sunlight to degrade three dyes (CV, CR, RBBR), the 50%-CPZH sunlight-enzymatic catalytic capacity was determined by monitoring the intensity change at the maximum absorbance of the three dyes using a UV-visible-near infrared spectrophotometer.[27] A video of sunlight catalytic dye degradation is shown in video S1 (ESI†).

Results and discussion

The X-ray diffraction (XRD) patterns of *x*%-CPZH are shown in Fig. 3a, and the XRD patterns of MA are shown in Fig. S1 (ESI†). The characteristic peaks at 2θ = 7.2°, 12.5°, 19.0°, 27.4° and 29.6° in Fig. 3a demonstrated that *x*%-CPZH matched well with the ZIF-90 and g-C_3N_4/PDI structures, while the introduction of HRP did not affect their crystal structures.[19,28] Among them, the peaks at 2θ = 19.0°, 27.4°, and 29.6° belonged to g-C_3N_4/PDI

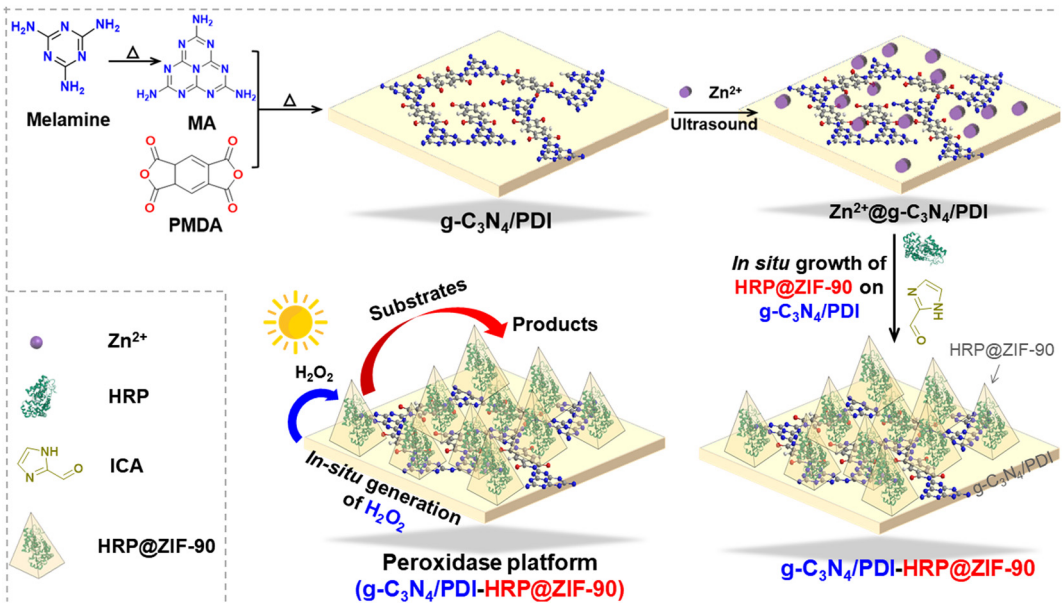

Fig. 2 Synthesis of g-C_3N_4/PDI-HRP@ZIF-90.

(2θ = 27.4° (002) and were due to g-C_3N_4 packing of the melem sheets, and the peaks at 2θ = 19.0° and 2θ = 29.6° were due to π,π-stacking of PDI units and donor–acceptor interactions between melem and PDI units).[29] The characteristic peaks of ZIF-90 were found at 2θ = 7.2° and 12.5° in *x*%-CPZH, indicating that ZIF-90 is tightly anchored to the g-C_3N_4/PDI two-dimensional structure, and the intensity of the characteristic peak of ZIF-90 was gradually enhanced with increasing input.[30]

As with all photoperoxidase cascade catalytic systems, the amount of H_2O_2 generated *in situ* by the photocatalyst directly influenced the catalytic activity of peroxidase. Too little H_2O_2 was unable to sustain the catalytic reaction of the peroxidase, and too much H_2O_2 damaged the catalytic active center of the peroxidase.[31–33] In order to select the best CPZH ratio, the activity of the ABTS oxidation model reactions was compared. As shown in Fig. 3b, with the increase in the ZIF-90 amount, the catalytic activity of CPZH gradually increased, peaking at 50%, and then decreased substantially at 100%; hence, subsequent characterization, stability and activity tests were carried out with 50%-CPZH.

Thermogravimetric analysis (TGA) was carried out (Fig. 3c) to determine the actual load amount of ZIF-90 in the 50%-CPZH product. The total weight loss of ZIF-90 at 0–800 °C was 76%, corresponding to the structural decomposition of ZIF-90, producing stable ZnO, which was consistent with the calculated weight loss of 68% (the error was caused by the residual solvent in ZIF-90). The weight loss of g-C_3N_4/PDI is 100% from 0–800 °C, which is related to the complete sublimation of this material. The weight loss of 50%-CPZH was more similar to that of g-C_3N_4/PDI, while 50%-CPZH lost 94.6% in the temperature range, and the residual mass was related to the *in situ* growth of ZIF-90 on the surface of g-C_3N_4/PDI. In comparison with g-C_3N_4/PDI, the mass loss of 50%-CPZH was 5.4% less, which can be matched to the original feeding ratio by calculation.

The FT-IR spectra of g-C_3N_4/PDI, ZIF-90, HRP and 50%-CPHZ are illustrated in Fig. 3d. The composite exhibits the characteristic peaks of g-C_3N_4/PDI at 807 cm^{-1}, 1000–1800 cm^{-1}, 1772 cm^{-1}, 1716 cm^{-1} and 726 cm^{-1} due to the high addition of g-C_3N_4/PDI in 50%-CPZH.[23,29] The vibrations of the composite at 2800–3200 cm^{-1} were caused by the aromatic and aliphatic C–H in ZIF-90, while the characteristic bands at 600–1500 cm^{-1} were related to the stretching and bending of the imidazole ring in ZIF-90.[22,34] In addition, the small peaks at 1400–1600 cm^{-1} and 2800–3000 cm^{-1} in 50%-CPZH were caused by the –CONH and $-CH_2$/$-CH_3$ groups in HRP.[35,36] Overall, FT-IR demonstrated that 50%-CPZH was a composite of g-C_3N_4/PDI, ZIF-90 and HRP, which agreed with the XRD results.

The elemental composition and chemical environment of 50%-CPZH, g-C_3N_4/PDI, and ZIF-90 were investigated by XPS analysis. As shown in Fig. 4a, the scanning spectra demonstrated the presence of C, O, N and Zn in 50%-CPZH. In contrast, the intensity of N in 50%-CPZH was stronger than that in ZIF-90, indicating that the hybridization of g-C_3N_4/PDI and ZIF-90 was successful, and the percentage weights of atoms in g-C_3N_4/PDI, ZIF-90, and 50%-CPZH are shown in Table S1 (ESI†). This result was generally consistent with the weight content of g-C_3N_4/PDI and ZIF-90 added during 50%-CPZH synthesis.[37] The C 1s spectra are illustrated in Fig. 4b, in which 50%-CPZH was found to exhibit four peaks at 287.8 eV, 287 eV, 286.1 eV, and 284.8 eV. C–C/C=C and C–N(O) at 284.8 eV and 286.1 eV were obtained by ZIF-90 and g-C_3N_4/PDI, respectively; $C-(N)_3$ at 287.8 eV was obtained by g-C_3N_4/PDI, due to the interaction of Zn^{2+} in ZIF-90 with N in g-C_3N_4/PDI, $C-(N)_3$ in 50%-CPZH has a slight negative shift; and C=N at 287.0 eV was obtained from the combination of g-C_3N_4/PDI and ZIF-90.

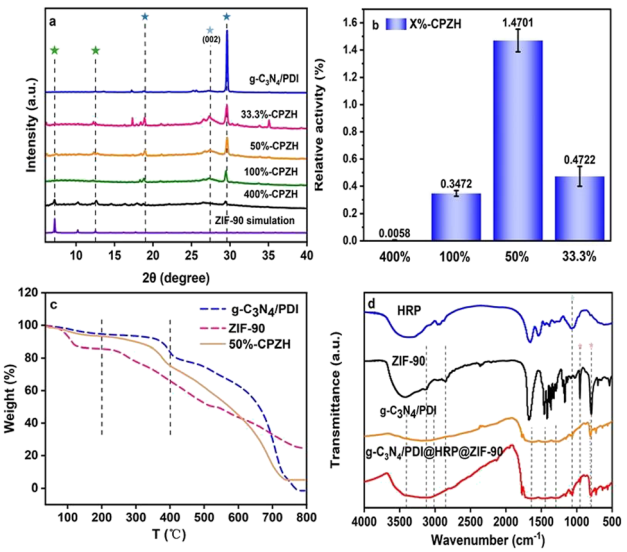

Fig. 3 (a) PXRD patterns of g-C_3N_4/PDI, ZIF-90 (simulated) and *x*%-CPZH; (b) comparison of the catalytic activity for *x*%-CPZH; (c) thermogravimetric analysis (TGA) for g-C_3N_4/PDI, ZIF-90 and 50%-CPZH; (d) FT-IR spectra of HRP, g-C_3N_4/PDI, ZIF-90 and 50%-CPZH.

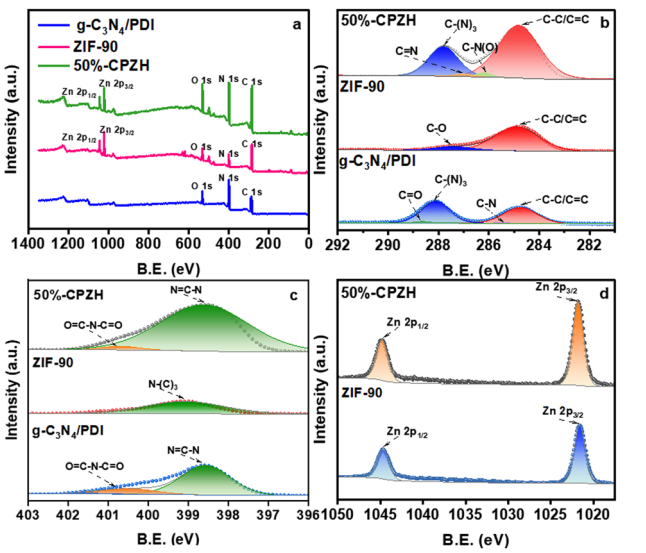

Fig. 4 (a) XPS survey spectra of ZIF-90, 50%-CPZH and g-C_3N_4/PDI; the corresponding high-resolution XPS spectra of (b) C 1 s and (c) N 1 s for ZIF-90, 50%-CPZH and g-C_3N_4/PDI; (d) high-resolution XPS spectra of Zn 2p for ZIF-90 and 50%-CPZH.

The N 1 s peak of 50%-CPZH (Fig. 4c) can be deconvoluted into two constituent peaks, which were assigned to N═C–N (398.6 eV) and O═C–N–C═O (400.7 eV). The XPS spectra of Zn 2p are displayed in Fig. 4d, with two peaks located at 1021.6 eV and 1044.7 eV, confirming the presence of Zn^{2+} in the 50%-CPZH structure. Compared to that of ZIF-90, the presence of g-C_3N_4/PDI in 50%-CPZH caused the electron density of Zn^{2+} to decrease, causing a positive shift in its binding energy. All these results further indicate that in 50%-CPZH, g-C_3N_4/PDI and ZIF-90 were not simply physically mixed but formed a heterojunction.[38]

The morphologies of g-C_3N_4/PDI, ZIF-90@HRP, and 50%-CPZH were characterized by SEM. The 2D sheet structures of g-C_3N_4/PDI and the sodalite structure of ZIF-90@HRP are shown in Fig. 5a and b. Many small sodalite structures can be observed in Fig. 5c, which proves that ZIF-90@HRP was *in situ* grown on g-C_3N_4/PDI. To further reveal the distribution of HRP and the structure of 50%-CPZH, FITC (fluorescein isothiocyanate)-labeled HRP and super-resolution confocal microscopy were used.

The spatial distribution of HRP in 50%-CPZH was evaluated by super-resolution confocal microscopy, and the structure of 50%-CPZH was analyzed by *Z*-axis sectioning (Fig. 5d–i).[39,40] Sliced at 0.5 μm intervals, the material cut at 0 μm was g-C_3N_4/PDI without luminescence, and the strongest luminescence was cut at 1 μm to the middle of ZIF-90@HRP. Due to the sodalite structure of ZIF-90@HRP, the luminescence intensity at 0.5 μm and 1.5 μm was weaker than that at 1 μm. The above results demonstrate that 50%-CPZH is a "semiconductor + MOF + peroxide" platform with g-C_3N_4/PDI as a substrate for the *in situ* growth of ZIF-90@HRP on the outer layer and that HRP was homogenously encapsulated in 50%-CPZH. This result agrees with the previous verification.

The above characterization of the material structure demonstrates that 50%-CPZH is a composite material with a g-C_3N_4/PDI substrate and ZIF-90 anchoring to the surface, meanwhile HRP is encapsulated in the interior with ZIF-90. We considered that the introduction of ZIF-90 would have a dual modulatory effect. On the one hand, it is possible to form heterojunctions between ZIF-90 and g-C_3N_4/PDI to improve the photoelectric properties of the semiconductor, enhancing the visible light utilization of the 2nd-generation "semiconductor + peroxidase" catalytic system. On the other hand, the restriction of the HRP tertiary structure *via* the framework of ZIF-90 improved the stability and recyclability of the 2nd-generation "semiconductor + peroxidase" catalytic system. Furthermore, the introduction of ZIF-90 has the potential to improve the compatibility of the two systems in terms of molecular transfer rate and catalytic environmental synergy.

We demonstrate the modulation effect by the introduction of ZIF-90 on the optical properties of the 2nd generation "semiconductor + peroxidase" system by comparing the activity of 50%-CPZH and g-C_3N_4/PDI with HRP mixtures (without ZIF-90) in catalyzing the ABTS oxidation reaction. As shown in Fig. 6a, the ZIF-90-free experimental group failed to respond to visible light at $\lambda > 420$ nm to produce sufficient H_2O_2 to excite the peroxidase to catalyze the half-reactive oxidation of ABTS.[41]

As shown in Fig. 6b, although HRP@ZIF-90 was physically mixed with g-C_3N_4/PDI at the same ratio as 50%-CPZH, the

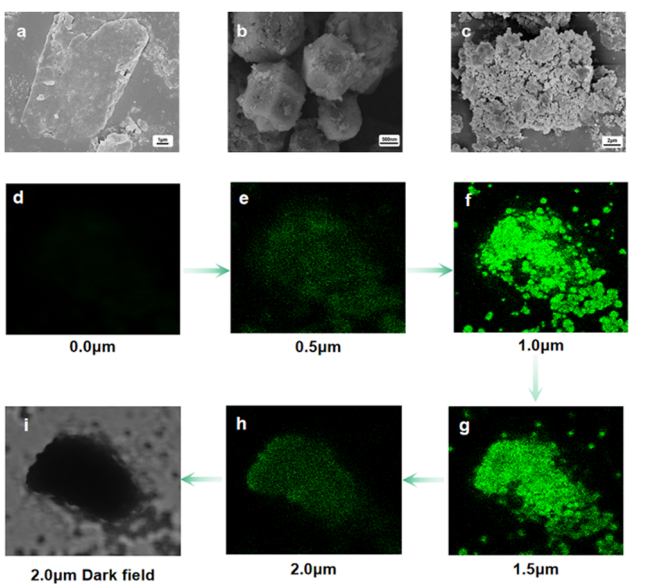

Fig. 5 SEM for (a) g-C_3N_4/PDI, (b) ZIF-90 and (c) 50%-CPZH; super-resolution confocal microscope *Z*-axis slices of 50%-CPZH (d–i). Video files have been included in the ESI.†

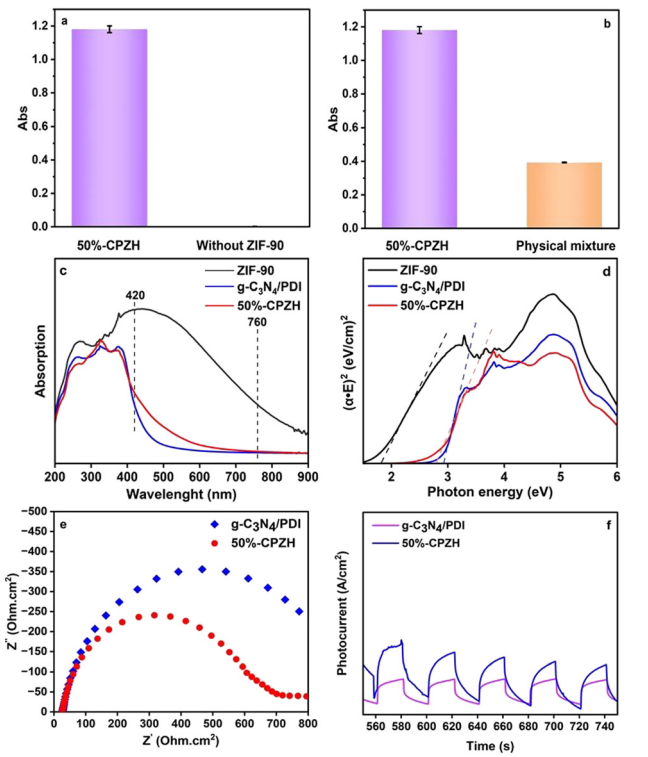

Fig. 6 (a) Comparison of the catalytic activity of 50%-CPZH and the catalyst without ZIF-90; (b) the catalytic activity of 50%-CPZH and a physical mixture of g-C_3N_4/PDI and HRP was compared; (c) UV-visible-near infrared spectra and (d) plot of $(\alpha hv)^2$ *vs.* photon energy for g-C_3N_4/PDI, ZIF-90 and 50%-CPZH; (e) EIS Nyquist plots and (f) transient photocurrent responses for g-C_3N_4/PDI and 50%-CPZH.

reaction efficiency of the physically mixed group was not as efficient as 50%-CPZH under the same catalytic conditions. It is related to the *in situ* anchoring of ZIF-90 on the g-C_3N_4/PDI surface, which shortens the shuttle distance of cofactor H_2O_2 between the photo-peroxidase catalytic modules and has a higher contact surface and homogeneity. Then we explain these phenomena by using UV-vis absorption spectra, EIS and photocurrent testing.[42]

The optical response of all samples was tested by obtaining the UV-vis absorption spectra. As shown in Fig. 6c, the main absorbance range of g-C_3N_4/PDI was less than 420 nm. In contrast, the introduction of ZIF-90 allowed 50%-CPZH to exhibit a wider absorption range and stronger absorption intensity in the visible range. Therefore, the composite 50%-CPZH has visible light absorption, demonstrating that the introduction of ZIF-90 enhances the use of photo energy.[43]

To reveal the effect of light absorption properties on the photocatalyst activity, the E_g of the catalyst was calculated by the Kubelka–Munk function: $(\alpha h\nu)1/n = A(h\nu - E_g)$. From the Tauc image (Fig. 6d), it is shown that the band gap energy of 50%-CPZH is 2.77 eV, which is less than that of g-C_3N_4/PDI (2.91 eV). This further confirms that the introduction of ZIF-90 is beneficial in reducing the band gap and thus enhancing the optical response.[44]

Furthermore, we verified the effect of the introduction of ZIF-90 on the optical properties of g-C_3N_4/PDI by electrochemical tests, and we evaluated the resistance of the photocatalysts using electrochemical impedance spectroscopy (EIS). Fig. 6e demonstrates that the Nyquist arc radius of 50%-CPZH is significantly smaller than that of g-C_3N_4/PDI, which indicates that the introduction of ZIF-90 effectively reduces the electron transfer resistance within the material and facilitates the migration of photogenerated carriers, which can effectively enhance the photocatalytic reaction performance.

In Fig. 6f, photocurrent tests have shown that the photocurrent intensity of 50%-CPZH is stronger than g-C_3N_4/PDI under 300 W Xe lamp irradiation at $\lambda > 420$ nm, which can be attributed to the introduction of ZIF-90 to effectively enhance the charge transfer capability.[45] The above data indicate that the *in situ* anchoring of ZIF-90 effectively enhances the electron–hole separation efficiency, electron transfer resistance and visible light utilization of the photocatalytic half-reaction in the 2nd generation "semiconductor – peroxidase" catalytic system.

The introduction of ZIF-90 into the 2nd generation "semiconductor + peroxidase" catalytic system not only enhances the catalytic efficiency of the photocatalytic half-reaction, but we consider that the introduction of ZIF-90 also greatly improves the stability and reusability of the enzymatic half-reaction. This is because the ZIF-90 crystals grow tightly around the HRP in 50%-CPZH forming a cavity structure that confines the HRP inside its cavity. This restriction effectively reduces the structural changes in the tertiary structure of HRP, and even inactivation, owing to external environmental variables. We have exposed the composite 50%-CPZH to adverse conditions to maintain the enzymatic structure. Then we verify the effect of the introduction of ZIF-90 on the stability and recyclability of the 2nd generation "semiconductor + peroxidase" catalytic system by comparing the reaction product concentrations.[46]

The sensitivity of pH is an inherent defect of the free-state enzyme, limiting its ability to be used industrially. Enzymes exhibit the greatest activity in the optimum pH range; above or below the optimum pH, the tertiary structure of the enzyme will be altered or even collapsed, which was the primary reason for the low free-state enzyme activity at extreme pH. As shown in Fig. 7a, the lower the pH, the higher the H^+ concentration in the catalytic environment and the more beneficial the H_2O_2 generation. Therefore, the optimum pH for the photocatalytic generation of H_2O_2 from g-C_3N_4/PDI-ZIF-90 was 3. The optimal HRP catalysis was at pH = 6, which is related to the HRP tertiary structure. The optimal catalytic conditions for the two systems are not compatible.[47]

However, as illustrated in Fig. 7b, 50%-CPZH has been exposed to an acidic environment and the trend of its catalytic activity was similar to the g-C_3N_4/PDI photocatalytic generation of H_2O_2. This is attributed to the framework restriction protection of ZIF-90 which reduced the destruction of HRP's tertiary structure in acidic environments and improved its acidic stability, allowing for increased compatibility between enzymatic and photocatalyzed half-reactive systems. Compared to the free-state HRP optimum catalytic pH = 6, 50%-CPZH optimum catalytic pH = 3 provides a basis for the industrial application of peroxidase.[48]

The catalytic function of the enzyme is mainly dependent on the enzyme's tertiary structure, which is partly maintained by the hydrogen bonding structure within the enzyme molecule. With increased temperature, the hydrogen bonds are gradually broken until the tertiary structure of the enzyme molecule is completely destroyed, which is the reason for enzyme inactivation due to high temperatures. The structural restrictive protection of HRP by ZIF-90 in 50%-CPZH was highlighted with increasing temperature, and when the temperature increased to 60 °C, 50%-CPZH still

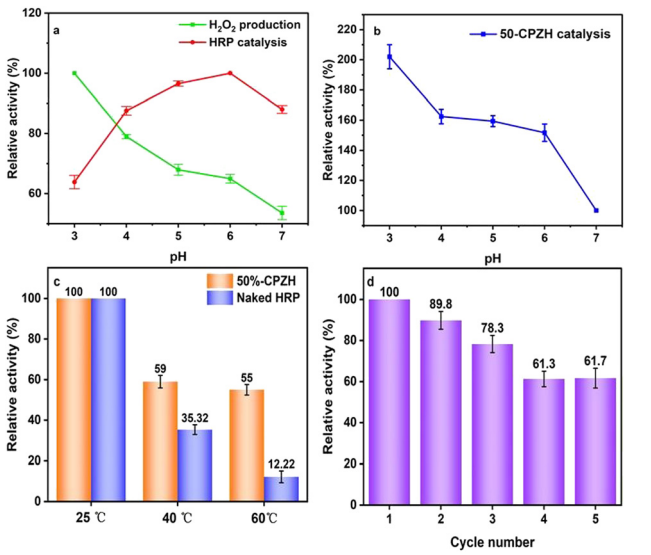

Fig. 7 (a) A comparison of g-C_3N_4/PDI-ZIF-90 photocatalytic production of H_2O_2 and HRP catalytic activity at pH 3–7; (b) the relative catalytic activity of 50%-CPZH at pH = 3–7; (c) comparison of the stability of 50%-CPZH and HRP at different temperatures; (d) the reusability of 50%-CPZH.

exhibited 55% relative activity, whereas HRP only exhibited 12.22% (Fig. 7c).[49]

Reusability is an important indicator for enzyme industrial applications, and excellent reusability can facilitate the formation of a continuously operating system for an enzyme to be used in industrial fixed or fluidized bed reactors. However, free-state HRP is water-soluble and difficult to separate from the reaction system after the reaction, thus significantly increasing the cost of enzyme industrial applications. In 50%-CPZH, HRP was confined by the solid carrier material ZIF-90 and anchored to the water-insoluble g-C_3N_4/PDI solid surface, allowing it to be easily separated from the mixed system after the reaction. As seen in Fig. 7d, 50%-CPZH can be reused at least 5 times, and the relative activity remains at 62%. The reduction in activity was due to mass loss during repeated isolation (the initial input amount was 10 mg, and after the fifth cycle, it remained at 5.43 mg).[50]

The above experimental results demonstrate our initial assumption that the introduction of ZIF-90 improves the optical utilization of the photocatalytic half-reactions; the enzyme stability and reusability of the enzymatic half-reactions of the 2nd generation "semiconductor + peroxidase" catalytic system. And due to the spatial limitation of ZIF-90, the compatibility between the photocatalytic and enzymatic half-reaction systems was enhanced in two ways (1) shortening the distance from the photocatalyzed generated H_2O_2 to the peroxidase active center; (2) coordinating the incompatibility between the photocatalytic production H_2O_2 optimal catalytic environment and the enzyme optimal catalytic environment. The introduction of ZIF-90 enhances the possibility for industrial catalysis of green biomanufacturing by using peroxidases in three aspects: photocatalytic half-reaction, enzyme-catalyzed half-reaction, and photoperoxidase full–reaction. We consider that the 50%-CPZH catalytic platform can directly utilize sunlight *in situ* generated H_2O_2 to stimulate peroxidase-catalyzed reactions and is not affected by the adverse effects of outdoor sunlight irradiation on the reaction system. Thus, we verified the above assumptions by degrading three dyes (CV, CR, RBBR) with real outdoor sunlight.

According to Fig. 8a, in the 50%-CPZH, g-C_3N_4/PDI modified by ZIF-90 is stimulated by sunlight to produce *in situ* generated H_2O_2, which diffuses through the pores of ZIF-90 into the internal cavity where HRP is encapsulated and reacts with resting HRP *via* a two-electron oxidation reaction to produce HRP I. HRP I then oxidized the dyes diffusing into the ZIF-90 interior through two single-electron reduction reactions, returning to the resting state in preparation for the next catalytic cycle.[51] According to Fig. 8b–d, the 50%-CPZH completely degraded all three dyes (CV, CR, RBBR) within 30 minutes, whereas the degradation capacity of g-C_3N_4/PDI + HRP (without ZIF-90 addition) was much weaker. It was associated with ZIF-90 to enhance g-C_3N_4/PDI optical utilization and adapt HRP to the external environment.

ZIF-90 was introduced to improve the stability of peroxidase and modify the optical properties of the semiconductor photocatalyst, enabling the original "semiconductor photocatalyst + peroxidase" system to obtain catalytic products directly from sunlight without being affected by the actual environment. This is a guiding role for the industrial application of peroxidase. It is attractive to replace HRP with other specific peroxidases to obtain more valuable compounds directly catalyzed by sunlight in extreme catalytic environments.

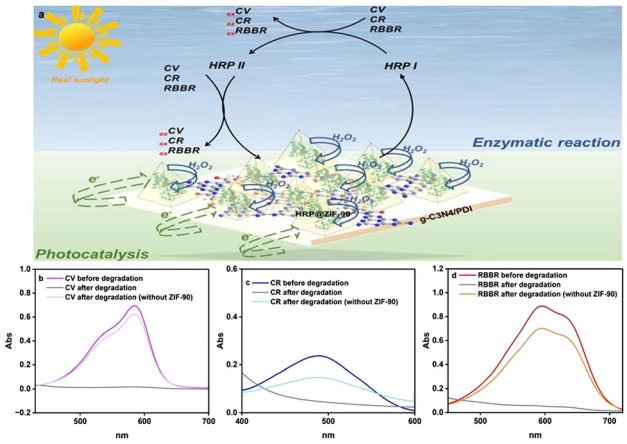

Fig. 8 (a) The mechanism of 50%-CPZH degradation of dyes; absorption spectra showing (b) CV, (c) CR, and (d) RBBR degradation under sunlight by 50%-CPZH and g-C_3N_4/PDI + HRP (without ZIF-90).

Conclusions

A new composite catalyst (photo-peroxidase platform) has been successfully designed and constructed. Photoperoxidase cascade reactions can be driven by using this platform in the visible light range of $\lambda > 420$ nm without the need for precious metals. In addition, the platform has demonstrated excellent reusability (more than 5 times), stability under extreme conditions (at pH = 3, catalytic activity was twice that at pH = 7) and practicality (all three dyes degrade rapidly in real sunlight). Due to the above results, the platform is capable of significantly reducing the drawbacks associated with the use of peroxidase-catalyzed reactions, and provides a suitable reference for the industrial application of peroxidases. This platform was supposed to provide potential for all peroxidases: the direct use of sunlight to catalyze more meaningful reactions under industrial conditions.

Author contributions

Ke-Xin Li: methodology, formal analysis, investigation, validation. Guo-Wei Guan: formal analysis, investigation, validation. Ling-Min Pei: supervision, writing – review & editing, funding acquisition. Qing-Yuan Yang: supervision, writing – original draft, writing – review & editing, project administration, funding acquisition.

Conflicts of interest

There are no conflicts to declare.

Acknowledgements

This work was financially supported by the National Natural Science Foundation of China (No. 21901198). Qing-Yuan Yang

acknowledges the Thousand Talents Programs of Shanxi Province. Ling-Min Pei acknowledges the Natural Science Foundation of Tibet Autonomous Region (XZ202001ZR0066G) and the Young Scholar Incubation Plan of Xizang Minzu University (22MDX02). We thank Mr Chang Huang at the Instrument Analysis Center of Xi'an Jiaotong University for their assistance with PXRD analysis.

Notes and references

1 Y. Ryu, J. A. Berry and D. D. Baldocchi, What is global photosynthesis? History, uncertainties and opportunities, *Remote Sens. Environ.*, 2019, **223**, 95–114.
2 Y. Tachibana, L. Vayssieres and J. R. Durrant, Artificial photosynthesis for solar water-splitting, *Nat. Photonics*, 2012, **6**, 511–518.
3 S. K. Wu, R. Snajdrova, J. C. Moore, K. Baldenius and U. T. Bornscheuer, Biocatalysis: Enzymatic Synthesis for Industrial Applications, *Angew. Chem., Int. Ed.*, 2021, **60**, 88–119.
4 T. L. Poulos, Heme enzyme structure and function, *Chem. Rev.*, 2014, **114**, 3919–3962.
5 R. Morsi, M. Bilal, H. M. N. Iqbal and S. S. Ashraf, Laccases and peroxidases: The smart, greener and futuristic biocatalytic tools to mitigate recalcitrant emerging pollutants, *Sci. Total Environ.*, 2020, **714**, 136572.
6 Y. Y. Sun, I. Sinev, W. Ju, A. Bergmann, S. Dresp, S. Kühl, C. Spöri, H. Schmies, H. Wang, D. Bernsmeier, B. Paul, R. Schmack, R. Kraehnert, B. Roldan Cuenya and P. Strasser, Efficient Electrochemical Hydrogen Peroxide Production from Molecular Oxygen on Nitrogen-Doped Mesoporous Carbon Catalysts, *ACS Catal.*, 2018, **8**, 2844–2856.
7 L. Zhou, J. R. Feng, B. C. Qiu, Y. Zhou, J. Y. Lei, M. Y. Xing, L. Z. Wang, Y. B. Zhou, Y. D. Liu and J. L. Zhang, Ultrathin g-C_3N_4 nanosheet with hierarchical pores and desirable energy band for highly efficient H_2O_2 production, *Appl. Catal., B*, 2020, **267**, 118396.
8 B. T. Nicholls, D. G. Oblinsky, S. I. Kurtoic, D. Grosheva, Y. X. Ye, G. D. Scholes and T. K. Hyster, Engineering a Non-Natural Photoenzyme for Improved Photon Efficiency, *Angew. Chem., Int. Ed.*, 2022, **61**, e202113842.
9 Y. C. Wang, H. Liu, Q. Y. Pan, C. Y. Wu, W. B. Hao, J. Xu, R. Z. Chen, J. Liu, Z. B. Li and Y. J. Zhao, Construction of Fully Conjugated Covalent Organic Frameworks via Facile Linkage Conversion for Efficient Photoenzymatic Catalysis, *J. Am. Chem. Soc.*, 2020, **142**, 5958–5963.
10 H. L. Hou, X. K. Zeng and X. W. Zhang, Production of Hydrogen Peroxide by Photocatalytic Processes, *Angew. Chem., Int. Ed.*, 2020, **59**, 17356–17376.
11 Y. Shiraishi, S. Kanazawa, Y. Sugano, D. Tsukamoto, H. Sakamoto, S. Ichikawa and T. Hirai, Highly Selective Production of Hydrogen Peroxide on Graphitic Carbon Nitride (g-C_3N_4) Photocatalyst Activated by Visible Light, *ACS Catal.*, 2014, **4**, 774–780.
12 X. K. Zeng, Y. Liu, Y. Kang, Q. Y. Li, Y. Xia, Y. L. Zhu, H. L. Hou, M. H. Uddin, T. R. Gengenbach, D. H. Xia, C. Sun, D. T. McCarthy, A. Deletic, J. Yu and X. Zhang, Simultaneously Tuning Charge Separation and Oxygen Reduction Pathway on Graphitic Carbon Nitride by Polyethylenimine for Boosted Photocatalytic Hydrogen Peroxide Production, *ACS Catal.*, 2020, **10**, 3697–3706.
13 M. Bilal, M. Asgher, R. Parra-Saldivar, H. B. Hu, W. Wang, X. H. Zhang and H. M. N. Iqbal, Immobilized ligninolytic enzymes: An innovative and environmental responsive technology to tackle dye-based industrial pollutants - A review, *Sci. Total Environ.*, 2017, **576**, 646–659.
14 Z. Ashkan, R. Hemmati, A. Homaei, A. Dinari, M. Jamlidoost and A. Tashakor, Immobilization of enzymes on nanoinorganic support materials: An update, *Int. J. Biol. Macromol.*, 2021, **168**, 708–721.
15 X. Zhao, T. Yang, D. Wang, N. Zhang, H. Yang, X. Jing, R. Niu, Z. Yang, Y. Xie and L. Meng, Gold Nanorods/Metal–Organic Framework Hybrids: Photo-Enhanced Peroxidase-Like Activity and SERS Performance for Organic Dyestuff Degradation and Detection, *Anal. Chem.*, 2022, **94**, 4484–4494.
16 B. L. Chen, X. Wang, X. Gao, J. Jiang, M. C. Hu, S. N. Li, Q. G. Zhai and Y. C. Jiang, DNA directed immobilization of horseradish peroxidase on phase-transitioned lysozyme modified TiO_2 for efficient degradation of phenol in wastewater, *Mater. Des.*, 2021, **201**, 109463.
17 E. Bilgin Simsek and D. Saloglu, Exploring the structural and catalytic features of lipase enzymes immobilized on g-C_3N_4: A novel platform for biocatalytic and photocatalytic reactions, *J. Mol. Liq.*, 2021, **337**, 116612.
18 Y. L. Guo, L. L. Yang, C. X. Zhao, Z. D. Gao, Y. Y. Song and P. Schmuki, Constructing a photo-enzymatic cascade reaction and it's in situ monitoring: enzymes hierarchically trapped in titania meso-porous MOFs as a new photosynthesis platform, *J. Mater. Chem. A*, 2021, **9**, 14911–14949.
19 Y. Y. Li, Y. Fang, Z. L. Cao, N. J. Li, D. Y. Chen, Q. F. Xu and J. M. Lu, Construction of g-C3N4/PDI@MOF heterojunctions for the highly efficient visible light-driven degradation of pharmaceutical and phenolic micropollutants, *Appl. Catal., B*, 2019, **250**, 150–162.
20 X. Yuan, S. L. Qu, X. Y. Huang, X. G. Xue, C. L. Yuan, S. W. Wang, L. Wei and P. Cai, Design of core-shelled g-C_3N_4@ZIF-8 photocatalyst with enhanced tetracycline adsorption for boosting photocatalytic degradation, *Chem. Eng. J.*, 2021, **416**, 129148.
21 M. Q. Qiu, Z. X. Liu, S. Q. Wang and B. Hu, The photocatalytic reduction of U(VI) into U(IV) by ZIF-8/g-C_3N_4 composites at visible light, *Environ. Res.*, 2021, **196**, 110349.
22 F. K. Shieh, S. C. Wang, C. I. Yen, C. C. Wu, S. Dutta, L. Y. Chou, J. V. Morabito, P. Hu, M. H. Hsu, K. C. Wu and C. K. Tsung, Imparting functionality to biocatalysts via embedding enzymes into nanoporous materials by a de novo approach: size-selective sheltering of catalase in metal-organic framework microcrystals, *J. Am. Chem. Soc.*, 2015, **137**, 4276–4279.
23 W. B. Liang, H. S. Xu, F. Carraro, N. K. Maddigan, Q. W. Li, S. G. Bell, D. M. Huang, A. Tarzia, M. B. Solomon, H. Amenitsch, L. Vaccari, C. J. Sumby, P. Falcaro and C. J. Doonan, Enhanced

Activity of Enzymes Encapsulated in Hydrophilic Metal-Organic Frameworks, *J. Am. Chem. Soc.*, 2019, **141**, 2348–2355.

24 Q. Liu, N. Y. Wang, J. Caro and A. S. Huang, Bio-inspired polydopamine: a versatile and powerful platform for covalent synthesis of molecular sieve membranes, *J. Am. Chem. Soc.*, 2013, **135**, 17679–17682.

25 Q. Chen, C. Liang, X. Q. Sun, J. W. Chen, Z. J. Yang, H. Zhao, L. Z. Feng and Z. Liu, H_2O_2-responsive liposomal nanoprobe for photoacoustic inflammation imaging and tumor theranostics via in vivo chromogenic assay, *Proc. Natl. Acad. Sci. U. S. A.*, 2017, **114**, 5343–5348.

26 T. T. Man, C. X. Xu, X. Y. Liu, D. Li, C. K. Tsung, H. Pei, Y. Wan and L. Li, Hierarchically encapsulating enzymes with multi-shelled metal-organic frameworks for tandem biocatalytic reactions, *Nat. Commun.*, 2022, **13**, 305.

27 Q. Y. Li, Z. P. Guan, D. Wu, X. G. Zhao, S. Y. Bao, B. Z. Tian and J. L. Zhang, Z-Scheme BiOCl-Au-CdS Heterostructure with Enhanced Sunlight-Driven Photocatalytic Activity in Degrading Water Dyes and Antibiotics, *ACS Sustainable Chem. Eng.*, 2017, **5**, 6958–6968.

28 F. S. Liao, W. S. Lo, Y. S. Hsu, C. C. Wu, S. C. Wang, F. K. Shieh, J. V. Morabito, L. Y. Chou, K. C. Wu and C. K. Tsung, Shielding against Unfolding by Embedding Enzymes in Metal-Organic Frameworks via a de Novo Approach, *J. Am. Chem. Soc.*, 2017, **139**, 6530–6533.

29 Y. Shiraishi, S. Kanazawa, Y. Kofuji, H. Sakamoto, S. Ichikawa, S. Tanaka and T. Hirai, Sunlight-driven hydrogen peroxide production from water and molecular oxygen by metal-free photocatalysts, *Angew. Chem., Int. Ed.*, 2014, **53**, 13454–13459.

30 S. Bhattacharjee, Y.-R. Lee and W. S. Ahn, Post-synthesis functionalization of a zeolitic imidazolate structure ZIF-90: a study on removal of Hg(ii) from water and epoxidation of alkenes, *CrystEngComm*, 2015, **17**, 2575–2582.

31 L. P. Wang, Y. Meng, C. X. Zhang, H. B. Xiao, Y. L. Li, Y. M. Tan and Q. J. Xie, Improving Photovoltaic and Enzymatic Sensing Performance by Coupling a Core-Shell Au Nanorod@TiO_2 Heterostructure with the Bioinspired l-DOPA Polymer, *ACS Appl. Mater. Interfaces*, 2019, **11**, 9394–9404.

32 Z. R. Wang, R. F. Zhang, X. Y. Yan and K. L. Fan, Structure and activity of nanozymes: Inspirations for de novo design of nanozymes, *Mater. Today*, 2020, **41**, 81–119.

33 J. Dumanovic, E. Nepovimova, M. Natic, K. Kuca and V. Jacevic, The Significance of Reactive Oxygen Species and Antioxidant Defense System in Plants: A Concise Overview, *Front. Plant Sci.*, 2020, **11**, 552969.

34 C. H. Wang, X. L. Liu, N. Keser Demir, J. P. Chen and K. Li, Applications of water stable metal-organic frameworks, *Chem. Soc. Rev.*, 2016, **45**, 5107–5134.

35 J. H. Zhu, Y. G. Feng, A. J. Wang, L. P. Mei, X. Luo and J. J. Feng, A signal-on photoelectrochemical aptasensor for chloramphenicol assay based on 3D self-supporting AgI/Ag/BiOI Z-scheme heterojunction arrays, *Biosens. Bioelectron.*, 2021, **181**, 113158.

36 L. J. Shaw, R. Blankstein, J. J. Bax, M. Ferencik, M. S. Bittencourt, J. K. Min, D. S. Berman, J. Leipsic, T. C. Villines, D. Dey, S. Al'Aref, M. C. Williams, F. Lin, L. Baskaran, H. Litt, D. Litmanovich, R. Cury, U. Gianni, I. Van den Hoogen, M. Budoff, H. J. Chang, E. H. H. G. Feuchtner, A. Ahmadi, B. B. Ghoshajra, D. Newby, Y. S. Chandrashekhar and J. Narula, Society of Cardiovascular Computed Tomography/North American Society of Cardiovascular Imaging - Expert Consensus Document on Coronary CT Imaging of Atherosclerotic Plaque, *J. Cardiovasc. Comput. Tomogr.*, 2021, **15**, 93–109.

37 X. F. Li, W. Q. Huang, X. Q. Liu and H. Bian, Graphene oxide assisted ZIF-90 composite with enhanced n-hexane vapor adsorption capacity, efficiency and rate, *J. Solid State Chem.*, 2019, **278**, 120890.

38 S. W. Liu, F. Chen, S. Li, X. X. Peng and Y. Xiong, Enhanced photocatalytic conversion of greenhouse gas CO_2 into solar fuels over g-C_3N_4 nanotubes with decorated transparent ZIF-8 nanoclusters, *Appl. Catal., B*, 2017, **211**, 1–10.

39 Z. J. Xu, G. T. Liu, J. Huang and J. Wu, Novel Glucose-Responsive Antioxidant Hybrid Hydrogel for Enhanced Diabetic Wound Repair, *ACS Appl. Mater. Interfaces*, 2022, **14**, 7680–7689.

40 A. A. P. Mansur, H. S. Mansur and S. M. Carvalho, Engineered hybrid nanozyme catalyst cascade based on polysaccharide-enzyme-magnetic iron oxide nanostructures for potential application in cancer therapy, *Catal. Today*, 2022, **388**, 187–198.

41 M. Raaja Rajeshwari, S. Kokilavani and S. Sudheer Khan, Recent developments in architecturing the g-C_3N_4 based nanostructured photocatalysts: Synthesis, modifications and applications in water treatment, *Chemosphere*, 2022, **291**, 132735.

42 X. Q. Wei, X. Wang, Y. Pu, A. N. Liu, C. Chen, W. X. Zou, Y. L. Zheng, J. S. Huang, Y. Zhang, Y. C. Yang, M. Naushad, B. Gao and L. Dong, Facile ball-milling synthesis of CeO_2/g-C_3N_4 Z-scheme heterojunction for synergistic adsorption and photodegradation of methylene blue: Characteristics, kinetics, models, and mechanisms, *Chem. Eng. J.*, 2021, **420**, 127719.

43 Q. H. Liang, X. J. Liu, J. J. Wang, Y. Liu, Z. F. Liu, L. Tang, B. B. Shao, W. Zhang, S. X. Gong, M. Cheng, Q. Y. He and C. Y. Feng, In-situ self-assembly construction of hollow tubular g-C_3N_4 isotype heterojunction for enhanced visible-light photocatalysis: Experiments and theories, *J. Hazard. Mater.*, 2021, **401**, 123355.

44 X. F. Li, J. F. Zhang, Y. Huo, K. Dai, S. W. Li and S. F. Chen, Two-dimensional sulfur-and chlorine-codoped g-C_3N_4/CdSe-amine heterostructures nanocomposite with effective interfacial charge transfer and mechanism insight, *Appl. Catal., B*, 2021, **280**, 119452.

45 R. C. Shen, K. L. He, A. P. Zhang, N. Li, Y. H. Ng, P. Zhang, J. Hu and X. Li, In-situ construction of metallic Ni_3C@Ni core–shell cocatalysts over g-C_3N_4 nanosheets for shell-thickness-dependent photocatalytic H_2 production, *Appl. Catal., B*, 2021, **291**, 120104.

46 S. Arana-Pena, D. Carballares, R. Morellon-Sterlling, A. Berenguer-Murcia, A. R. Alcantara, R. C. Rodrigues and R. Fernandez-Lafuente, Enzyme co-immobilization: Always the biocatalyst designers' choice…or not?, *Biotechnol. Adv.*, 2021, **51**, 107584.

47 W. Liang, P. Wied, F. Carraro, C. J. Sumby, B. Nidetzky, C. K. Tsung, P. Falcaro and C. J. Doonan, Metal-Organic Framework-Based Enzyme Biocomposites, *Chem. Rev.*, 2021, **121**, 1077–1129.
48 A. Basso and S. Serban, Industrial applications of immobilized enzymes—A review, *Mol. Catal.*, 2019, **479**, 110607.
49 K. X. Li, Q. Y. Yang, P. P. Zhang and W. Y. Zhang, Research Progress of Peroxygenase-Catalyzed Reactions Driven by in-situ Generation of H_2O_2, *Chin. J. Org. Chem.*, 2022, **42**, 732–741.
50 S. R. Yousefi, H. A. Alshamsi, O. Amiri and M. Salavati-Niasari, Synthesis, characterization and application of Co/Co_3O_4 nanocomposites as an effective photocatalyst for discoloration of organic dye contaminants in wastewater and antibacterial properties, *J. Mol. Liq.*, 2021, **337**, 116405.
51 H. An, J. Song, T. Wang, N. Xiao, Z. Zhang, P. Cheng, S. Ma, H. Huang and Y. Chen, Metal-Organic Framework Disintegrants: Enzyme Preparation Platforms with Boosted Activity, *Angew. Chem., Int. Ed.*, 2020, **59**, 16764–16769.